Compound Size Effect in Composite Beams with Softening Connectors. I: Energy Approach

By Zdeněk P. Bažant,[1] Fellow, ASCE, and Jan L. Vítek[2]

ABSTRACT: The size effect on the nominal strength of steel-concrete composite beams caused by shear failures of connectors such as welded studs is analyzed by two different approaches: (1) In this paper (Part I) by a fracture type analysis of the energy release caused by propagation of the zone of failed connectors along the beam; and (2) in a companion paper (Part II) by a direct solution of the load-deflection diagrams from the differential equations of beam bending theory. The former can capture the large size asymptotic size effect and yields simple formulas suitable for design, whereas the latter can provide the solution for small beam sizes for which the connector failure zone is not much shorter than the span. The force-slip diagram of the connectors exhibits postpeak softening, which engenders an energetic size effect on the nominal strength of the connector. If the connectors are geometrically scaled with the beam, the size effect in the shear failure of connectors (mesoscale) is superimposed on the size effect due to propagation of the zone of connector failures along the beam (macroscale), producing in the beam as a whole a compound size effect that is stronger than in linear elastic failure mechanics. If the connector sizes and the interface area per connector are not scaled with the overall dimensions of the composite beam, the size effect law proposed by Bažant in 1984 is applicable. Comparisons with available test results are presented in Part II.

INTRODUCTION

Composite beams consisting of a steel beam and a concrete slab [Fig. 1 (top)] are often used in bridges and buildings. Crucial components are the connectors between the concrete slab and the steel beam. They usually consist of welded steel studs embedded in concrete.

A composite beam may fail by tensile yielding of steel, compression crushing of the concrete slab, or slip of the connectors. Designing against the first two modes of failure is well understood. The last mode failure is more complicated and will be the focus of this paper.

In the classical approach to composite beam analysis [e.g., Johnson (1994)], the connectors have been considered as elastoplastic. This would imply the absence of size effect and the presence of a long yield plateau on the load-deflection diagram of the beam after the maximum force has been reached. The following five observations, however, indicate that the behavior of the connectors is usually brittle, or more precisely quasi-brittle, and that a size effect on the nominal strength of composite beam must be expected:

1. Many valuable experimental studies of composite beams have been conducted (McMackin et al. 1973; Oehlers and Coughlan 1986; Eligehausen and Ožbolt 1990; Wright and Francis 1990; Eligehausen et al. 1992; Oehlers and Park 1992; Rehm et al. 1992; Eligehausen and Zhao 1993; Oehlers and Sved 1995). However, none of them clarifies the postpeak softening and the size effect on nominal strength. The evaluation of test results assumed plastic behavior a priori, which precludes size effect. Most measurements stopped at, or shortly after, the maximum load. This is, of course, understandable because large enough loading frames that would be sufficiently stiff to stabilize postpeak softening of the composite beam are generally unavailable and would be very expensive. One must nevertheless note that if the composite beam did not exhibit postpeak softening, it would have been easy to continue the tests into large deflections. This fact means that, in the tests that have stopped at peak load, the presence of postpeak softening intense enough to destabilize the test must be suspected.

2. Those few laboratory tests that progressed somewhat beyond the peak load exhibited postpeak softening that was rather mild (and thus did not require an extremely stiff loading frame). As is now well understood, however [e.g., Bažant and Chen (1997); Bažant and Planas (1998); and Bažant (1999)], a mild softening for a small laboratory structure implies steep softening for a large structure, which in turn implies size effect.

3. Studs designed strong enough to remain elastic fail due to formation of large cracks in the concrete slab. This is generally a brittle type of failure exhibiting a strong size effect, which should be manifested by a size effect in the failure of the whole composite beam.

4. The pullout failure of anchors is now known to be rather brittle, exhibiting a strong energetic size effect, almost as strong as that in linear elastic fracture mechanics (LEFM).

5. Recent tests by Kuhlmann and Breuninger (1998) revealed that the shear failure of studs embedded in concrete exhibits a very pronounced postpeak softening (Fig. 2), except when a heavy 3D reinforcement is used. Even though tests of different sizes have not been made, one must nevertheless conclude that the stud failures ought to exhibit a size effect on their nominal strength and that the larger the stud, the steeper must be the postpeak softening. A further necessary consequence is that the studs in the beam cannot reach their maximum shear force simultaneously. In other words, the stud failures must propagate along the beam, which is a fracture-type behavior calling for energy release analysis. Furthermore, it follows that a size effect on the strength of both the studs and the composite beam as a whole is inevitable.

The objective of this two-part article is to use the beam bending theory to approximately calculate the size effect and postpeak softening of composite beams caused by the softening behavior of connectors. Two rather different approaches will be taken: (1) In this paper (Part I), a fracture mechanics-
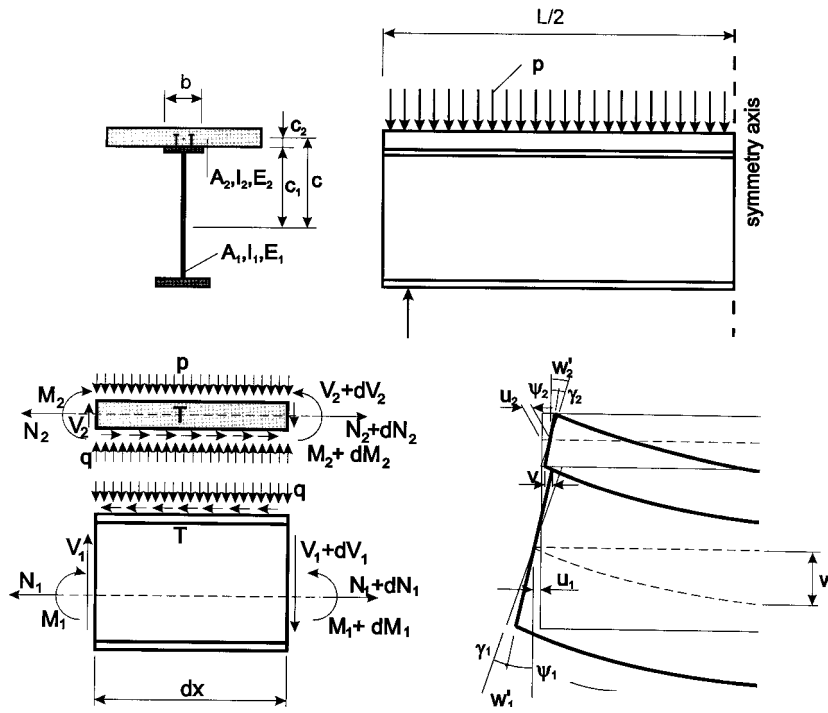
FIG. 1.   (Top) Composite Beam and Its Cross Section; (Bottom) Internal Forces and Displacements
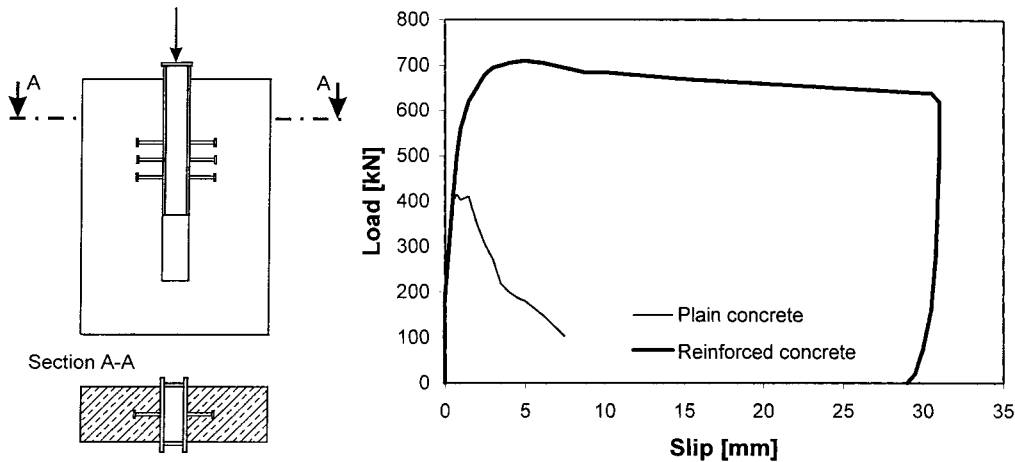

FIG. 2.   Selected Test Results of Kuhlmann and Breuninger (1998) Revealing Existence of Postpeak Softening of Studs Embedded in Plain or Three-Dimensionally Reinforced Concrete Blocks (Embedment in Slabs with Typical Reinforcement May Be Assumed Intermediate between the Two Cases Shown by Curves)

type analysis of the energy release, the basic ideas of which have been summarized at a recent conference (Bažant and Vítek 1998); and (2) in a companion paper [Part II (Bažant and Vítek 1999)], a solution of the differential equations of the problem. The former is simple and asymptotically exact for very large beam sizes but can be too crude for normal sizes. The latter is more accurate for small sizes for which the zone of failing connectors is not small compared with the span but is more complicated and not amenable to simple design formulas.

It might be objected by some that the beam bending theory is too simple to resolve the stress concentrations near the front of the propagating zone of connector failures. Simple though this theory indeed is, it nevertheless does predict satisfactorily the overall energy release from the whole beam, which is the crucial variable for fracture propagation. The physical meaning of the stress intensity factor is not a measure of the stress singularity, which in reality does not exist, but a measure of the overall energy release rate into the fracture front. Therefore, it is not necessary to consider in beams a 2D stress field with a singularity. Indeed, if the structure consists of beams,

the bending theory is known to give stress intensity factors that are asymptotically exact as slenderness tends to infinity.

FORCE-SLIP DIAGRAM OF CONNECTORS

First, we need to characterize the behavior of connectors, including the postpeak and the size effect on nominal strength. Many experimental and theoretical investigations have clarified various aspects of the behavior of shear connectors and composite beams (Ollgaard et al. 1971; McMackin et al. 1973; Oehlers and Coughlan 1986; Oehlers 1989; Eligehausen and Ožbolt 1990; Wright and Francis 1990; Johnson and Molenstra 1991; Maruyama et al. 1991; Eligehausen et al. 1992; Oehlers and Park 1992; Rehm et al. 1992; Eligehausen and Zhao 1993; Johnson 1994; Leon and Deierlein 1995; Oehlers and Sved 1995; Kuhlmann and Breuninger 1998). However, apparently the only study that provides at least some experimental information on the postpeak softening behavior of shear-loaded studs is that of Kuhlmann and Breuninger (1998). However, shear-loaded studs of different sizes that would be geometrically similar, to reveal the size effect on the nominal shear
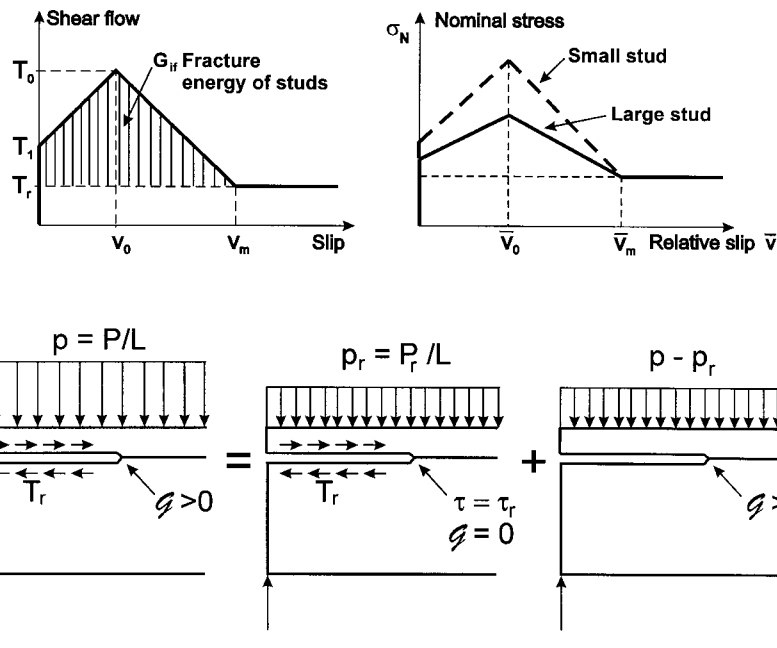
FIG. 3. (Top Left) Idealized Shear Force-Slip Diagram of Deformable Connectors; (Top Right) Size Effect on Nominal Stress; (Bottom) Beam with Equivalent Interface Cracks Subjected to Residual Tractions and Decomposition into Two Loading Cases According to Principle of Superposition ($p_r = P_r/L$ = Distributed Load Corresponding to P_r)

strength of the stud, have unfortunately not been tested by any of these investigators.

The size effect and post-postpeak softening were theoretically analyzed by Bažant and Vítek (1994) who developed an approximate energy-based model. According to this analysis, the diagram of the shear flow T (shear force per unit length of interface) versus the slip v is approximated as piecewise linear (Fig. 3). In the case of the first (virgin) loading, the diagram begins with an initially vertical segment representing an increase of shear force without any slip. In the case of repeated loading, the initial perfect bond (represented by shear force development without any slip) no longer exists, and so the diagram begins with a finite slope. However, this is not the case when a repeated load is superposed on a significant dead load, as is typical of bridges.

The second linear segment is a simplification of a rising curve leading to the peak (ultimate) value F_u of shear flow T. The first two linear segments of the diagram have been experimentally calibrated by Bažant and Vítek (1994) using the data of Eligehausen and Zhao (1993). The third linear segment, approximately describing postpeak softening, was predicted theoretically, on the basis of energy arguments (Bažant and Vítek 1994). The last, fourth linear segment is introduced to describe frictional slip at constant stress equal to the residual shear strength, whose value might be finite. The theoretical prediction of the postpeak softening shear response of studs is qualitatively verified by the very recent test results of Kuhlmann and Breuninger (1998) (Fig. 2).

The postpeak decrease of stud force represents softening damage. Such damage is generally known to localize into a finite zone, called the fracture process zone (Bažant and Planas 1998). This zone propagates during failure along the beam. Therefore, the limit capacity of different connectors is not mobilized simultaneously, as assumed in plastic limit analysis. One must expect the softening to occur only in a limited group of connectors that occupies a certain finite length l_c and propagates during loading along the steel-concrete interface. This is a fracture-type behavior. Because the softening is defined by a stress-displacement rather than stress-strain relation, l_c normally is approximately constant, independent of the beam size. Consequently, a size effect must be expected.

Palmer's and Rice's J-integral analysis (1973) of similar shear fracture problems of rock mechanics shows that the area lying under the stress-displacement curve and above the horizontal line corresponding to the asymptotic shear stress value (Fig. 3) represents the fracture energy G_{if} of the interface per unit area. This result renders possible a simple approximate energy analysis of the size effect.

BASIC CONCEPT AND NOTATION

The objective now is to determine the effect of propagation of a softening failure of deformable connectors on the stress distribution along a simply supported beam and on the deflections of the beam as a whole. Except for the softening of connections, the formulation is similar to that presented by Newmark et al. (1952) and reviewed by Johnson (1994). Assuming the beam and slab to be sufficiently slender, they can be described by 1D theory of bending. This means that the shear lag is neglected. The 2D behavior of wide slabs may nevertheless be approximately taken into account by means of an effective width. Creep, shrinkage, and thermal effects are beyond the scope of this study.

The failure of a composite beam may be caused by failure of (1) the steel beam; (2) the concrete slab; or (3) the connection. Our interest lies in the last cause of failure, which implies the material in neither the beam nor the slab to be failing. Small parts of the beam or the slab might get plasticized or develop cracking before the connection fails. However, even if that is the case, the assumption of elastic behavior outside the interface is acceptable overall. The reason is that, during fracture propagation, the structure releases its stored energy into the fracture process zone as the material undergoes unloading, and the unloading is always elastic.

The assumption of elastic behavior outside the interface, of course, does not imply the load-deflection diagram to be elastic. The propagation of failure along the interface makes this diagram highly curved. This curvature has in previous studies been routinely attributed to plasticity but doubtless it is caused mainly by the propagating interface failure, provided the third cause of failure applies (we do not analyze here the failures that are not caused by nonyielding connectors).

It is, therefore, acceptable to consider the behavior of steel and concrete as elastic. This assumption requires further discussion in the case in which concrete undergoes cracking (smeared cracking is assumed here). Obviously, the linearity of concrete is fully justified if all the concrete lies within the compression zone of the cross section (i.e., if the neutral axis lies within the steel beam). This is normal for bridge beams, for which the slab is relatively thin in comparison with the height of the beam. In the case of composite beams typical of building structures, the neutral axis usually lies in the concrete slab (whose relative thickness is larger than in bridges, being approximately 1/3 of the height of the beam). If the usual no-tension assumption is adopted for the concrete slab and if the neutral axis does not move significantly during connection failure, the assumption of elastic behavior in the concrete slab is still justified, as an approximation. The cracking of the slab is thus taken into account by an equivalent reduced slab thickness.

Fig. 1(bottom left) shows an element of the composite beam. Let c_1 and c_2 be distances of the steel-concrete interface from the centroids of the steel beam and the concrete slab, both taken as positive [Fig. 1(top)]; $y = e_1$ and $y = e_2$ are the y-coordinates of the centroids of the beam and slab from the centroid of the transformed composite cross section (y being measured from this centroid), $e_1 > 0$, $e_2 < 0$; $Z_i = E_i A_i$ = axial stiffness of the concrete and steel parts; $R_i = E_i I_i$ = elastic bending stiffnesses; $S_i = E_i A_{si}$ = elastic shear stiffnesses (i = 1 for beam and 2 for slab); and A_{si} = cross section areas A_i after correction for nonuniformity of shear stress distribution.

A vertical distributed load p (per unit length of beam) is applied on the concrete slab. The deformations are characterized by deflection w, which is common to both parts of the cross section, slip v between steel and concrete, axial displacements u_1 in the steel beam centroid and u_2 in the concrete slab centroid, and cross section rotations ψ and γ of beam and slab [Fig. 1(bottom right)]. The total bending moment, normal force, and shear force transmitted by the whole cross section are denoted as M, N, and V, respectively. The interaction of the beam and slab is represented by shear flow F and vertical normal force q distributed along the interface. The steel and concrete parts transmit internal forces M_1, N_1, V_1 and M_2, N_2, V_2, respectively, and the shear flow (shear force per unit length) in the interface is denoted as T.

Although the present method can be applied to any composite beam, only the special case of a uniformly loaded simply supported symmetric beam is considered in what follows. The response is also assumed to be symmetric, even though it does not have to be (and almost certainly is not, due to inevitable imperfections). This is not only for the sake of simplicity. If a nonsymmetric response were analyzed, the results would be the same as long as the beam is statically determinate.

Because of the assumption of symmetry, the slip at midspan vanishes due to the symmetry and only half of the beam needs to be analyzed. For symmetric response, the problem is equivalent to that of a cantilever of length $L/2$.

ENERGY RELEASE FROM COMPOSITE BEAM

The failure loads of all quasi-brittle structures exhibit a deterministic size effect, which is understood as a dependence of the nominal strength of the structure σ_N on its size D (the characteristic dimension) when geometrically similar structures are compared. For similarity in three dimensions, $\sigma_N = P/D^2$, where P = maximum load. In the case of uniformly distributed load p, P is defined as the load resultant pD, and then $\sigma_N = p/D$. If the material failure criteria are expressed exclusively in terms of stresses and strains, as in plasticity, σ_N

is always independent of D; that is, there is no deterministic size effect (Bažant 1984, 1993).

In composite beams, one must expect a compound size effect representing a superposition of two separate size effects: (1) The size effect in the failure of the structure as a whole (macroscale), due to nonsimultaneous (propagating) failure of the connectors (mesoscale); and (2) another size effect in the failure of a substructure—the connectors (mesoscale), due to fracture growth around the stud (microscale). The easiest way to approximately determine this compound size effect is to analyze the energy release.

We consider a simply supported composite beam subjected to an arbitrarily distributed or concentrated load with a single load parameter P. The bending moment and shear force in the composite beam may be expressed in the form $M(x) = PDq(\xi)$ and $V(x) = Pq'(\xi)$, where P = load parameter, x = coordinate measured from the left end of the beam, $\xi = x/D$, $q(\xi)$ = some size-independent dimensionless function, $q'(\xi) = dq(\xi)/d\xi$, and $D = h$ = beam depth.

First, we assume, for the sake of simplicity, that there is a sharp (pointwise) transition from connectors that do not slip to connectors that carry the residual shear flow T_r. In other words, the zone of connector failures (analogous to the fracture process zone) is assumed to have a negligible length, as in LEFM. Thus we consider that there are two symmetrically located regions of length a (Fig. 4) such that for $x \leq a$ the shear flow T in the studs has been reduced to the residual shear flow value T_r (Fig. 3) and for $x > a$ there is no slip. In the sense of continuum smearing of the studs, these regions may be regarded as two symmetric sharp interface cracks subjected on their faces to tangential tractions T_r [Fig. 3(bottom left)].

The composite beam will be analyzed according to the theory of bending, in which the cross sections are assumed to remain plane, and the energy of shear stresses will be taken into account. The shear flow in the steel-concrete interface just ahead of the tip $x = a$ of these interface cracks (i.e., just ahead of the zone of slipped connectors) is given by the well-known formula

$$T(a, c_1) = \frac{V(a)Q_{tr}(c_1)}{I_{tr}} \tag{1}$$

where $T(a, c_1)$ = shear flow in the interface ($y = c_1$) just ahead of point $x = a$; I_{tr} = centroidal moment of inertia of the transformed cross section; and $Q_{tr}(c_1)$ = first (static) moment of inertia of the transformed area of concrete about the centroid of the transformed cross section.

Because $V(a) = Pq'(a)$, we may solve from (1) the load P_r for which $T(a, c_1) = T_r$ = residual value of the shear flow in the connectors at large slip

$$P_r = \frac{T_r I_{tr}}{Q_{tr}(c_1)q'(a)} \tag{2}$$

When the load has this value, the shear flow in the connection is continuous through the point $x = a$ and the energy release rate $\mathcal{G}$ due to extending the smeared equivalent interface cracks vanishes.
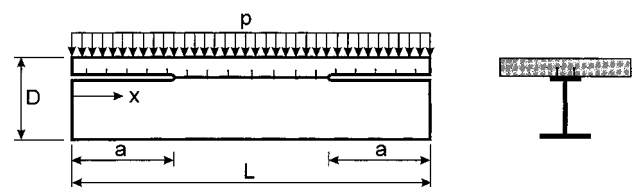
It is now convenient to imagine the solution for load P as

FIG. 4. Composite Beam with Studs Failed in Symmetric Crack-Like Regions of Length *a*

a superposition of the solutions for the following two loading cases [Fig. 3(bottom)]:

- A—The case with load value P_r (or corresponding distributed load p_r), for which the energy release rate $\mathcal{G} = 0$
- B—the case with load value $P - P_r$ (or distributed load $p - p_r$), for which the tangential tractions on the faces of the smeared equivalent interface cracks vanish

In loading case A, there is obviously no energy release into the tip of the equivalent crack ($\mathcal{G} = 0$) and thus no size effect, and $P = P_r$. In loading case B the energy release rate is nonzero and must be analyzed, which is what we do next. All of the size effect arises from this loading case.

The concrete and steel ahead of the crack tip act as a composite beam of bending stiffness

$$R = R_1 + R_2 + A_1 e_1^2 + A_2 e_2^2 \tag{3}$$

Behind the crack tip, the steel and concrete in loading case B behave as two separate beams forced to deflect equally (we assume the slab not to lift above the steel beam). Therefore, $M = M_1 + M_2$, and because the curvatures of the steel beam and the slab are equal, their bending moments (for $x < a$) are

$$M_1 = \frac{MR_1}{R_1 + R_2}; \quad M_2 = \frac{MR_2}{R_1 + R_2} \tag{4a,b}$$

respectively, and the bending energies per unit length of beam are $M_1^2/2R_1$ and $M_2^2/2R_2$.

Small though the contribution of shear strains may be, it is easy to take them into account. Although the Bernoulli-Navier hypothesis that cross sections remain plane and normal implies zero shear strains, it is known that deflection predictions of deep beams are improved by calculating the shear angles from the shear force V. This is a well-known, generally accepted paradox of the classical beam bending theory. For the region without stud failures (no interface crack), the shear angle is V/S, where S = shear stiffness of the composite cross section. This means that the complementary shear strain energy $V^2/2S$ per unit length of beam should be included for the region without interface crack.

In the region with stud failures (i.e., with interface crack), both parts of the beam undergo the same deflection w. Because $V = V_1 + V_2$ and the shear forces in parts 1 and 2 are $V_1 = R_1 d^3 w/dx^3$ and $V_2 = R_2 d^3 w/dx^3$, one finds that, for the classical bending theory and loading case B, the total shear force $V = V_1 + V_2$ distributes as

$$V_1 = V \frac{R_1}{R_1 + R_2}; \quad V_2 = V \frac{R_2}{R_1 + R_2} \tag{5a,b}$$

The complementary energies of the shear stresses per unit length of the cracked region of beam are $V_1^2/2S_1$ and $V_2^2/2S_2$.

Integration of the foregoing energy expressions yields the complementary potential energy of the left half of the composite beam

$$\Pi^* = \int_0^a \left(\frac{M_1^2}{2R_1} + \frac{M_2^2}{2R_2} + \frac{V_1^2}{2S_1} + \frac{V_2^2}{2S_2} \right) dx + \int_a^{L/2} \left(\frac{M^2}{2R} + \frac{V^2}{2S} \right) dx \tag{6}$$

where a = length of the crack (stud failure region). As known from fracture mechanics [e.g., Bažant and Planas (1998, Section 2.1.2)], the energy release rate due to growing a is obtained by differentiation with respect to a at constant load. Because the distribution of M and V does not depend on a (as the beam is statistically determinate)

$$\left[\frac{\partial \Pi^*}{\partial a} \right]_{P=\text{const}} = \left[\frac{M_1^2}{2R_1} + \frac{M_2^2}{2R_2} + \frac{V_1^2}{2S_1} + \frac{V_2^2}{2S_2} - \frac{M^2}{2R} + \frac{V^2}{2S} \right]_{x=a} \tag{7}$$

$$\left[\frac{\partial \Pi^*}{\partial a} \right]_{P=\text{const}} = \left[\frac{M^2}{2(R_1 + R_2)} + \frac{V^2}{2S_a} - \frac{M^2}{2R} + \frac{V^2}{2S} \right]_{x=a} \tag{8}$$

in which we inserted (4) and (5), and made the notation

$$\frac{1}{S_a} = \frac{R_1^2/S_1 + R_2^2/S_2}{(R_1 + R_2)^2} \tag{9}$$

Now, introducing dimensionless deflections by $M = (P - P_r)Dq(\xi)$, $V = (P - P_r)q'(\xi)$, and noting that the energy release rate must be equal to the energy consumed and dissipated by stud failures per unit length of the interface bG_{if}, one obtains

$$\left[\frac{\partial \Pi^*}{\partial a} \right]_{P=\text{const}} = \frac{[(P - P_r)Dq(\alpha)]^2}{2E_s D^4 \hat{R}} + \frac{[(P - P_r)q'(\alpha)]^2}{2E_s D^2 \hat{S}} = bG_{if} \tag{10}$$

with the notations

$$\frac{1}{\hat{R}} = E_s D^4 \left(\frac{1}{R_1 + R_2} - \frac{1}{R} \right); \quad \frac{1}{\hat{S}} = E_s D^2 \left(\frac{1}{S_a} - \frac{1}{S} \right) \tag{11a,b}$$

which are positive size-independent dimensionless parameters of the cross section geometry. The energy dissipation rate, analogous to the fracture energy may be expressed as $bG_{if} = G_{\text{stud}} n/s$, where G_{stud} = energy dissipated by slip of one stud [representing the cross-hatched area above the residual shear flow line in Fig. 3(top)], s = longitudinal spacing of studs; and n = number of rows of studs across the width of the interface strip.

ENERGETIC SIZE EFFECT

From (10) we may calculate the nominal stress corresponding to $P - P_r$ in loading case B

$$\sigma_N - \sigma_r = \frac{P - P_r}{D^2} = \frac{1}{Dq(\alpha)} \sqrt{\frac{2E_s G_{\text{stud}} n}{\{[q(\alpha)]^2 \hat{R}^{-1} + [q'(\alpha)]^2 \hat{Q}^{-1}\} s}} \tag{12}$$

Now it is necessary to introduce a reasonable assumption on the relative length of the stud failure zone [i.e., $\alpha = a/D$ (relative interface crack length)] in beams of different sizes D. From experience with many kinds of fracture (Bažant and Planas 1998), it may be assumed that, for a limited but significant range of sizes, the failures are geometrically similar; that is, the values of a/D at maximum load are the same for various sizes D. This assumption is indirectly justified by the fact that approximately the same size effect ensues by the solution of size effect from the differential equations of the problem presented later, which does not depend on this assumption. In this regard it may also be pointed out that no size effect would occur only if a were either vanishingly small or constant for various sizes, which is certainly not the case (or if all stud failures were simultaneous rather than propagating, which however cannot be the case because the studs exhibit postpeak softening).

The zone in which the studs are already slipping but their shear flow has not yet been reduced to T_r does not have a vanishing length (i.e., it is not a point). In reality, it occupies a certain finite length, which is denoted as $2c_0$. The behavior may be approximated by an effective (equivalent) sharp LEFM crack in the steel-concrete interface reaching roughly into the middle of the zone. This effective interface crack has the length $a = \alpha_0 D + c_0$, where $\alpha_0 = a_0/D$, and a_0 now represents the length in which the shear flow of the studs has been reduced to T_r.

By analogy with the size of the fracture process zone in quasi-brittle materials, we may consider c_0 and α_0 to be approximately constant (i.e., size independent). Now, substituting $\alpha = \alpha_0 + (c_0/D)$ into (12) we may conveniently introduce Taylor series expansions

$$q(\alpha) = q_0 + q_1(c_0/D) + (q_2/2)(c_0/D)^2 + \cdots \quad (13)$$

$$q'(\alpha) = q_1 + q_2(c_0/D) + (q_3/2)(c_0/D)^2 + \cdots \quad (14)$$

where constants $q_0 = q(\alpha_0)$, $q_1 = q'(\alpha_0)$, $q_2 = q''(\alpha_0)$, ... Thus we obtain

$$\sigma_N - \sigma_r$$

$$= \frac{1}{D}\sqrt{\frac{2(n/s)E_sG_{\text{stud}}}{[q_0 + q_1(c_0/D) + \cdots]^2\hat{R}^{-1} + [q_1 + q_2(c_0/D) + \cdots]^2\hat{S}^{-1}}} \quad (15)$$

We will now consider two basic geometrical types of scaling.

Type I

The composite beam is scaled in proportion to D, whereas the connection characteristics per unit area of steel-concrete interface remain constant (which would be the case for a glued interface with a crack). In that case, n/D, s, and G_{stud} are constant, and so are D/n and the transverse spacing of stud rows b/n. Then, if the series expansions are truncated after the first (linear) term, (15) can be rearranged to the form of the usual size effect law with residual stress (Bažant 1987) (see curve I in Fig. 5)

$$\sigma_N = \frac{\sigma_N^0}{\sqrt{1 + (D/D_0)}} + \sigma_r \quad (16)$$

in which

$$D_0 = c_0\frac{A_1}{A_2}; \quad \sigma_N^0 = \sqrt{\frac{2}{s}\left(\frac{n}{D}\right)\frac{E_sG_{\text{stud}}}{A_1c_0}} \quad (17a,b)$$

$$A_0 = \frac{q_0^2}{\hat{R}} + \frac{q_1^2}{\hat{S}}; \quad A_1 = 2q_1\left(\frac{q_0}{\hat{R}} + \frac{q_2}{\hat{S}}\right) \quad (18a,b)$$

Asymptotically, for very large D, (16) indicates that

$$\sigma_N - \sigma_r \propto \frac{1}{\sqrt{D}} \quad (19)$$

which is the scaling of LEFM.

Type II

In the second type of scaling, not only the composite beam but also the connectors and their spacing are geometrically scaled. In this case, representing the complete geometric scaling of the entire structure on both the macroscale of beam and the mesoscale of studs, one must take into account the effect of stud diameter d on the nominal strength of the stud. Because d is now proportional to beam depth D, this may be done by expressing the energy required for failure of the studs per unit length of the beam (the shaded area in Fig. 3) as follows:

$$G_{\text{stud}} = \pi d^2(\sigma_{N,\text{stud}} - \sigma_{r,\text{stud}})v_{\text{stud}} = (\sigma_{N,\text{stud}} - \sigma_{r,\text{stud}})D^2\bar{v}_{\text{stud}} \quad (20)$$

where $\bar{v}_{\text{stud}} = \pi(d/D)^2v_{\text{stud}}$ and d/D = constants; and $\sigma_{r,\text{stud}} = T_r/\pi d^2$ = residual nominal strength of stud. The constant v_{stud},
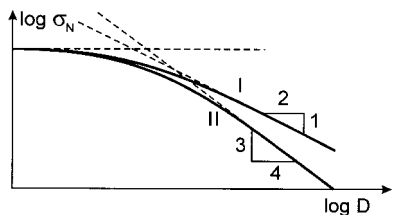

FIG. 5. Size Effects Predicted by Energy Release Analysis for Geometrical Scalings of Types I and II

independent of stud sizes, represents the effective slip displacement of stud characterizing its dissipated energy. The part of nominal strength of the stud that exceeds $\sigma_{r,\text{stud}}$ is subjected to size effect

$$\sigma_{N,\text{stud}} - \sigma_{r,\text{stud}} = \frac{\sigma_{s0}}{\sqrt{1 + (d/d_{s0})}} = \frac{\sigma_{s0}}{\sqrt{1 + (D/D_{s0})}} \quad (21)$$

where d_{s0} and D_{s0} = constants. From tests and finite-element studies [e.g., Eligehausen and Ožbolt (1992)], the pullout nominal strength is known to exhibit a very strong size effect, closely approaching the LEFM size effect $\sigma_{N,\text{stud}} \propto d^{-1/2}$. Therefore, it may be expected that, for practical stud sizes, $d/d_{s0} = D/D_{s0} \gg 1$, which means that $\sigma_{N,\text{stud}} \approx \sigma_{s0}\sqrt{D_{s0}/D}$ and that the residual nominal strength $\sigma_{r,\text{stud}}$ is negligible.

Using (20), (21), and (15), one obtains for size effect the law

$$\sigma_N = \sqrt{\sigma_{s0}\sigma_{b0}}\left(1 + \frac{D}{D_0}\right)^{-1/2}\left(1 + \frac{D}{D_{s0}}\right)^{-1/4} + \sigma_r \quad (22)$$

in which D_0 and σ_{b0} are constants

$$D_0 = c_0\frac{A_1}{a_0}; \quad \sigma_{b0} = \frac{2n}{A_1c_0}\left(\frac{D}{s}\right)E_s\bar{v}_{\text{stud}} \quad (23a,b)$$

For very large sizes D, this expression leads to the asymptotic size effect (curve II in Fig. 5)

$$\sigma_N - \sigma_r \propto D^{-3/4} \quad (24)$$

At first it may be unexpected that this size effect, which may be called the size hypereffect, is stronger than the LEFM size effect $D^{-1/2}$. The reason is that this is a compound size effect, in which the size effect due to failure of the beam as a whole (macroscale) is amplified by the size effect in the failure of individual studs (mesoscale).

Obviously, from the viewpoint of the size effect, when a larger composite beam is designed it is better not to increase the size of the studs, if possible. This is the normal design practice anyway. But unfortunately it is not feasible when the beam size is enlarged significantly. In that case, the stud size must be enlarged as well.

Note that if we analyzed the whole beam instead of its half, the results would be the same. Indeed, only the integral limit $L/2$ in (6) needs to be replaced by L, and if the beam is considered to fail nonsymmetrically, with stud failures advancing only on one side, (7) remains valid. If the beam is considered to fail symmetrically, with stud failures advancing on both sides, the expression in (7) must be multiplied by 2, but bG_{if} in (10) must be replaced by $2bG_{if}$. Although, according to path stability analysis (Bažant and Cedolin 1991, Sections 10.2 and 12.5), the nonsymmetric case is that which must occur, it does not matter because function $q(\xi)$ is independent of a if the beam is statistically determinate. For a statically indeterminate symmetric beam, though, different size effect expressions would result because $q(\xi)$ would also depend on a, causing a further term that would have to be added to (7).

Question of More Accurate Size Effect Law

Considering α in (12) to be constant is, admittedly, a simplification, albeit probably a good one. Eq. (12), however, is valid even if α depends on the structure size. It is obvious that this equation will still give a size-dependent nominal strength σ_N except if both $q(\alpha)$ and $q'(\alpha)$ were constant (i.e., independent of size D). This generally cannot happen except if α were 0 (i.e., if the composite beam were failing right when the first stud fails).

Thus it is clear that even without the hypothesis of size-independent α (i.e., without assuming geometric similarity of

failure states), a size effect must take place. Eq. (12) would provide a more accurate size effect law if the size dependence of α is determined, for example, experimentally.

CLOSING REMARKS

Although the energetic analysis of size effect in composite beams is instructive and simple, it is based on some simplifying hypotheses, particularly the hypothesis that the lengths of stud failure zones in beams of different sizes are geometrically similar. Therefore, it is of interest to also carry out a more accurate solution based on a direct solution of the differential equations. This is done in Part II, along with a comparison with the test data that exist.

APPENDIX I.   MULTIPLE LEVELS OF SCALED SUBSTRUCTURES

For a structure without a substructure, the strongest possible size effect is the LEFM size effect that is of the type $D^{-1/2}$. However, we have seen that a stronger deterministic size effect occurs when there is a brittle substructure. Consider now that there are n progressively refined subscales with quasi-brittle substructures. Perfect geometrical similarity occurs when the scaling ratio is the same for all the substructures. By extension of the argument that led to (22), it follows that the nominal strength obeys the following compound size effect:

$$\sigma_N - \sigma_r \propto \left(1 + \frac{D}{D_0}\right)^{-1/2} \left(1 + \frac{D}{D_1}\right)^{-1/4} \left(1 + \frac{D}{D_2}\right)^{-1/8}$$
$$\cdots \left(1 + \frac{D}{D_n}\right)^{-1/2^n} \tag{25}$$

where $D_0, D_1, D_3, \ldots, D_n$ = positive constants. The asymptotic scaling for very large D is

$$\sigma_N - \sigma_r \propto D^{2^{-1} + 2^{-2} + 2^{-3} + \cdots + 2^{-n}}; \quad \lim_{n \to \infty} (\sigma_N - \sigma_r) \propto 1/D \tag{26a,b}$$

APPENDIX II.   REFERENCES

Bažant, Z. P. (1984). "Size effect in blunt fracture: Concrete, rock, metal." *J. Engrg. Mech.*, ASCE, 110(4), 518–535.

Bažant, Z. P. (1987). "Fracture energy of heterogeneous material and similitude." Preprints, *Proc., SEM-RILEM Int. Conf. on Fracture of Concrete and Rock*, S. P. Shah and S. E. Swartz, eds., Society for Experimental Mechanics, 390–402.

Bažant, Z. P. (1993). "Scaling laws in mechanics of failure." *J. Engrg. Mech.*, ASCE, 119(9), 1828–1844.

Bažant, Z. P. (1999). "Size effect in structures: A review." *Archives of Mech. (Ingenieur-Archiv)*, Berlin, in press.

Bažant, Z. P., and Cedolin, L. (1991). *Stability of structures: Elastic, inelastic, fracture and damage theories*. Oxford University Press, New York.

Bažant, Z. P., and Chen, E.-P. (1997). "Scaling of structural failure." *Appl. Mech. Rev.*, 50(10), 593–627.

Bažant, Z. P., and Planas, J. (1998). *Fracture and size effect in concrete and other quasibrittle materials*. CRC, Boca Raton, Fla., and London.

Bažant, Z. P., and Vítek, J. L. (1994). "Stud connectors in composite beams: Simplified failure modeling and size effect." *Fracture and damage of quasibrittle structures*, Z. P. Bažant et al., eds., E & FN Spon, London, 331–341.

Bažant, Z. P., and Vítek, J. L. (1998). "Size effect in composite beams with deformable connections." *Proc., 3rd Int. Conf. on Fracture Mech. of Concrete Struct.*, H. Mihashi et al., ed., Aedificatio Publishers, Freiburg, Germany, 1537–1546.

Bažant, Z. P., and Vítek, J. L. (1999). "Compound size effect in composite beams with softening connectors. II: Differential equations and behavior." *J. Engrg. Mech.*, ASCE, 125(11), 1315–1322.

Eligehausen, R., Bouška, P., Červenka, V., and Pukl, R. (1992). "Size effect of the concrete cone failure load of anchor bolts." *Proc., Fracture Mech. of Concrete Struct., 1st Int. Conf.*, Z. P. Bažant, ed., Elsevier Science, London, 517–525.

Eligehausen, R., and Ožbolt, J. (1990). "Numerical analysis of headed studs embedded in large plain concrete blocks." *Proc., Computer Aided Analysis and Design of Concrete Structures, Int. Symp.*, B. Bićanić and H. Mang, eds., Pineridge, Swansea, U.K., 645–656.

Eligehausen, R., and Zhao, G. (1993). "Tragverhalten von randfernen Kopfbolzen unter Querlast." *Rep.*, Institut für Werkstoffe in Bauwesen, Universität Stuttgart, Stuttgart, Germany (in German).

Johnson, R. P. (1994). *Composite structures of steel and concrete*, Vol. 1. Blackwell Scientific, London.

Johnson, R. P., and Molenstra, N. (1991). "Partial shear connection in composite beams for buildings." *Proc., Inst. Civ. Engrs.* London, Part 2, 91, 679–704.

Kuhlmann, U., and Breuninger, U. (1998). "Zur Tragfähigkeit von horizontaler liegenden Kopfbolzdübeln." *Stahlbau*, Berlin, 67(7), 547–550 (in German).

Leon, R. T., and Deierlein, G. D. (1995). "An overview of codes, standards and guidelines for composite construction." *Restructuring: America and beyond*, 1297–1299.

Maruyama, K., Shimizu, K., and Momose, M. (1991). "Load carrying mechanism of anchor bolt." *Proc., IABSE Colloquium, IABSE Rep.*, Int. Assoc. for Bridge and Structural Engrg., Zürich, Vol. 62, 743–748.

McMackin, P. J., Slutter, R. G., and Fisher, J. W. (1973). "Headed steel anchor under combined loading." *AISC Engrg. J.*, 43–52.

Newmark, N. M., Siess, C. P., and Viest, I. M. (1952). "Studies of slab and beam highway bridges. Part III—Small scaled tests of shear connectors and composite T-beams." *Bull. 396*, University of Illinois, Urbana, Ill.

Oehlers, D. J. (1989). "Splitting induced by shear connectors in composite beams." *J. Struct. Engrg.*, ASCE, 115(2), 341–362.

Oehlers, D. J., and Coughlan, C. G. (1986). "The shear stiffness of stud-shear connections in composite beams." *J. Constr. Steel Res.*, 6(4), 273–284.

Oehlers, D. J., and Park, S. M. (1992). "Shear connectors in composite beams with longitudinally cracked slabs." *J. Struct. Engrg.*, ASCE, 118(8), 2004–2022.

Oehlers, D. J., and Sved, G. (1995). "Composite beams with limited-slip-capacity shear connectors." *J. Struct. Engrg.*, ASCE, 121(6), 932–938.

Ollgaard, J. R., Slutter, R. G., and Fisher, J. W. (1971). "Shear strength of stud connectors in lightweight and normal-weight concrete." *AISC Engrg. J.*, 55–64.

Palmer, A., and Rice, J. R. (1973). "The growth of slip surfaces in the progressive failure of over-consolidated clay." *Proc. of the Royal Society of London*, A332, 527–548.

Rehm, G., Eligehausen, R., and Mallée, R. (1992). *Betonkalender—Befestigungstechnik*. Ernst und Sohn, Berlin (in German).

Wright, H. D., and Francis, R. W. (1990). "Tests on composite beams with low levels of shear connection." *The Struct. Engr.*, London, 68(15/7), 293–298.

Compound Size Effect in Composite Beams with Softening Connectors. II: Differential Equations and Behavior

By Zdeněk P. Bažant,[1] Fellow, ASCE, and Jan L. Vítek[2]

ABSTRACT: After presenting an energy analysis of size effect in the first part of this study, the second part gives a solution by integrating the differential equations of beam bending theory, coupled with a softening force-slip law for the interface. This analysis is more accurate than the previous energy analysis but does not yield simple explicit formulas for the size effect. The results generally support the simple conclusion from energy analysis. They do not disagree with the available limited experimental evidence; however, measurements of size effect in geometrically scaled composite beams seem unavailable. Further tests are needed.

INTRODUCTION

After presenting the energy analysis of the size effect in Part I of this study (Bažant and Vítek 1999), attention in Part II is focused partly on a solution by integration of the differential equations of beam bending theory coupled with a softening stress-displacement law for slip at the interface between the steel beam and the concrete plate caused by shear loading of the steel connectors. All definitions and notations from Part I are retained.

PROBLEM FORMULATION IN TERMS OF DIFFERENTIAL EQUATIONS

We will now take a different approach—the direct solution of the differential equations provided by the beam bending theory. The differential equations of equilibrium of the steel beam are

$$M_1' - V_1 + Tc_1 = 0; \quad V_1' + q = 0; \quad N_1' - T = 0 \quad (1a\text{–}c)$$

and those of the concrete slab are

$$M_2' - V_2 + Tc_2 = 0; \quad V_2' + p - q = 0; \quad N_2' + T = 0 \quad (2a\text{–}c)$$

where the primes denote the derivatives d/dx (x = axial coordinate of beam) (e.g., $f' = df/dx$). The equations of equilibrium of the composite cross section are

$$M_1 + M_2 + N_1 c = M; \quad N_1 + N_2 = 0 \quad (3a,b)$$

where $c = c_1 + c_2$ = distance between the centroids of steel and concrete. The compatibility conditions read

$$v = u_1 + \psi_1 c_1 - (u_2 - \psi_2 c_2) \quad (4)$$

$$\psi_1 = w' - \frac{V_1}{S_1}; \quad \psi_2 = w' - \frac{V_2}{S_2} \quad (5a,b)$$

$$\psi_1' = -\frac{M_1}{R_1}; \quad \psi_2' = -\frac{M_2}{R_2} \quad (5c,d)$$

The shear flow as a function of the slip of the connection is shown in Fig. 3 in Part I. A linear relation is assumed for each segment of this idealized diagram. That is, for the prepeak segment, the shear flow thus is

---

[1]Walter P. Murphy Prof. of Civ. Engrg. and Mat. Sci., Northwestern Univ., Evanston, IL 60208. E-mail: z-bazant@nwu.edu

[2]Assoc. Prof., Czech Tech. Univ. (ČVUT), Prague, 16229 Czech Republic.

$$T = T_v v + T_1 \quad (6)$$

where $T_v = dT/dv$ = constant = slope of the second segment of the diagram, and T_1 = constant.

The foregoing equations represent a system of 14 differential and algebraic equations involving 14 unknown forces and displacements: M_1, M_2, V_1, V_2, N_1, N_2, T, q, u_1, u_2, ψ_1, ψ_2, w, and v.

SOLUTION OF DIFFERENTIAL EQUATIONS

The half-span of the beam [see Fig. 1(top) in Part I] may be divided into four intervals, corresponding to the four linear segments of the quadrilinear diagram in Fig. 3 of Part I governing the value of T_v in (6). The spatial coordinates x_1, x_2, and x_3 of the end points of the corresponding intervals of the diagram of shear flow versus slip along the beam are unknown, cannot be explicitly calculated in advance, and vary during the loading depending on the behavior of the whole beam. They may be calculated by an iterative solution of the beam. However, the discontinuity of the slope of the shear flow diagram T_v makes it difficult to satisfy the conditions at the boundary points between these intervals exactly.

To facilitate the solution, the shear strains in the beam and slab are neglected (i.e., $S_1 = S_2 \to \infty$). Then the system of differential equations can be reduced to one differential equation of the second order

$$v'' - \alpha Tc = -\frac{c}{R_1 + R_2} v \quad (7)$$

where α = coefficient depending on the stiffness of the beam

$$\alpha = \frac{(Z_1 + Z_2)(R_1 + R_2) + Z_1 Z_2 c^2}{Z_1 Z_2 c (R_1 + R_2)} \quad (8)$$

In the first of the aforementioned intervals ($0 \le x \le x_1$), the shear flow T is constant, having the value T_r. In the second interval ($x_1 < x \le x_2$), the shear flow increases from the value T_r to the peak value T_0. In the third interval ($x_2 < x \le x_3$), the shear flow decreases from T_0 to T_1. In the fourth interval ($x_3 < x < l/2$), the shear flow decreases to zero at the midspan. The slips at x_1, x_2, and x_3 are equal to v_m, v_0, and 0, respectively.

Two types of load control may be considered. For type 1, the loading is given as the input, and the response of the beam is to be calculated. In type 2, the slip at the end is given as the input, and the load and the response of the beam are to be calculated. Only for loading type 2 it is possible to obtain the descending (softening) part of the load-deflection diagram.

For loading type 1, the position of the coordinate x_3 can be calculated directly, because the load p is known from the conditions in which there is no slip in the fourth interval and in which the shear flow at x_3 is T_1

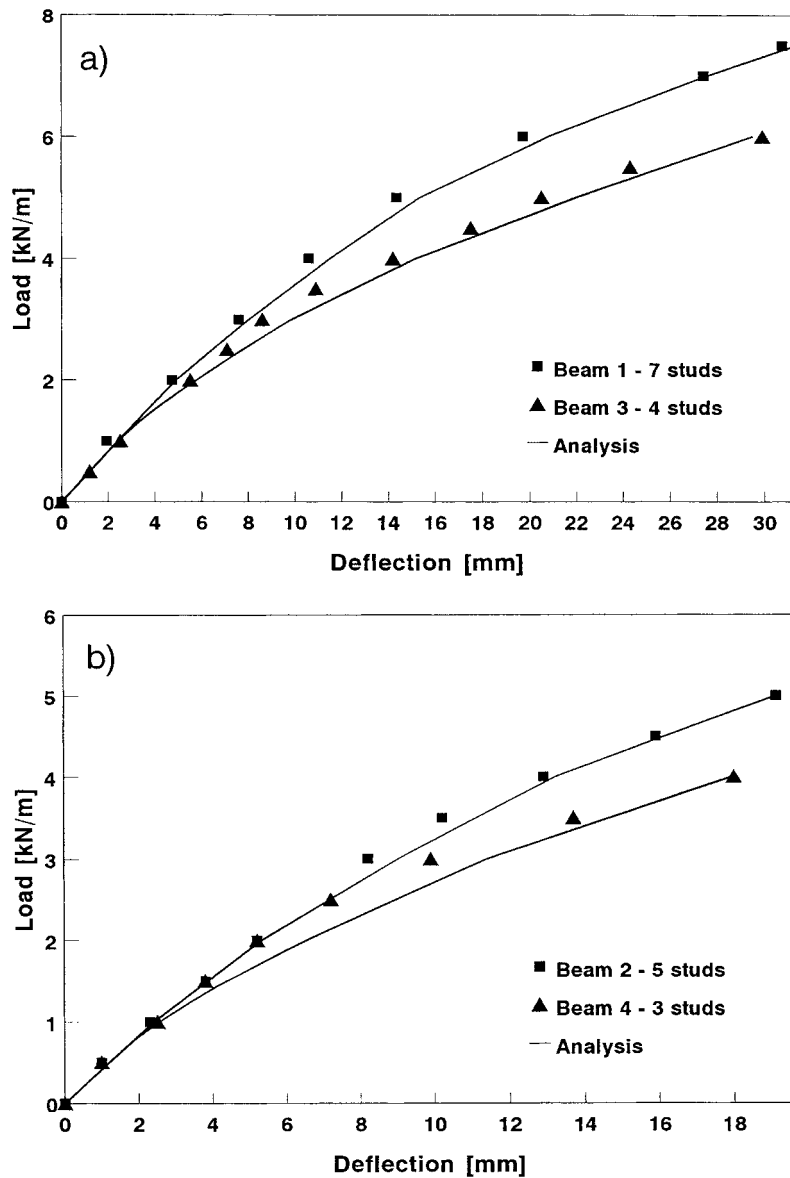$$x_3 = \frac{l}{2} - T_1 \frac{\alpha(R_1 + R_2)}{p} \quad (9)$$

FIG. 1. Load-Deflection Curve and Comparison of Analysis with Experiment: (a) Test Beams 1 and 3; (b) Test Beams 2 and 4

Coordinates x_1 and x_2 can be calculated from the additional conditions in which the curvature w'' of the beam is continuous through x_1 and through x_2.

The boundary conditions necessary to solve (7) are given for each interval separately. They also depend on the level of loading. Only at high loads may all four intervals be observed in the beam. At low loads, no slip occurs and point x_3 may appear outside the beam, which means it does not exist. At higher loads, points x_3 and x_2 occur within the beam, and at still higher loads, point x_1 also appears.

The boundary condition at the end of the beam is for all the stages $v'(0) = 0$. The boundary conditions at points x_1 and x_2 are $v(x_1) = v_m$ and $v(x_2) = v_0$. In interval 1 ($0 \leq x < x_1$), the solution is

$$v = \frac{-cp}{R_1 + R_2} \left[\frac{l}{4} (x^2 - x_1^2) - \frac{1}{6} (x^3 - x_1^3) \right] + \frac{\alpha T_r c}{2} (x^2 - x_1^2) + v_m \tag{10}$$

In interval 2 ($x_1 \leq x < x_2$)

$$v = c_1 \sin(\omega x) + c_2 \cos(\omega x) + \frac{1}{\omega^2} \left[\frac{cp(2x - l)}{2(R_1 + R_2)} + (T_0 + T_{v2}v_0)\alpha c \right] \tag{11}$$

where $\omega = \sqrt{T_{v2}\alpha c}$. In interval 3 ($x_2 \leq x < x_3$)

$$v = c_1 e^{\omega x} + c_2 e^{-\omega x} + \frac{1}{\omega^2} \left[\frac{cp(2x - l)}{2(R_1 + R_2)} + T_1 \alpha c \right] \tag{12}$$

where $\omega = \sqrt{T_{v3}\alpha c}$; and c_1, c_2, c_3, and c_4 = integration constants. In interval 4 ($x_3 \leq x \leq l/2$), $v = 0$.

For loading type 1, coordinate x_3 can be easily calculated, but it is not known in advance how many intervals will appear in the half-beam. Coordinates x_1 and x_2 need to be determined iteratively. The internal forces are calculated from (1)–(3) and (5). After calculating the curvature from (4), the cross section rotations and the deflections can be integrated.

For loading type 2, it is clear how many intervals will occur in the half-beam. On the other hand, x_3 is not known, because p is not known. Iterations are needed to calculate x_3.

ANALYSIS OF RESULTS

Comparison with Previous Experiments

The foregoing solution has been compared with the measurements of four beams tested by Wright and Francis (1990). The beams were 8 m long, consisting of a rolled steel I-beam

312.5 mm deep and a concrete slab reinforced by deformed bars, 115 mm thick and 2.5 m wide. The four beams differed in the stiffness of connection. Stud connectors were welded in one row at equal spacing along each beam. Beam No. 1 had seven studs (of diameter 19.0 mm, length 100 mm, and tensile strength 450 MPa), beam No. 2 had five studs, beam No. 3 had four studs, and beam No. 4 had only three studs per half-span. Concentrated loads were applied in four pairs, approximating a uniformly distributed load. The beams were first loaded dynamically (about 50% of the ultimate load), and then the load was raised monotonically to the ultimate load. The postpeak response could not be measured. First the connection failed, and then the concrete slab cracked and failed. The proposed simple analysis cannot model the detailed nonlinear response but can predict the failure of connection.

The ultimate load carried by each stud was determined according to the formulas derived by Bažant and Vítek (1994). Because the spacing of the studs is large enough compared with a fracture cone developed during stud failure, the forces of the individual studs can be simply superposed.

The data on the shear flow-slip diagram are presented in Table 1. The critical slips (v_0 and v_m) are the same for all the beams, but the vertical coordinates (T_1, T_0, and T_r) are multiplied by the number of studs per half-span. Because the tests were terminated well before the danger of collapse, the terminal points of the measured load-slip diagrams are not the maximum loads. The response has been calculated only up to these terminal slip values. From the comparison of the experimental and calculated results in Figs. 1(a and b), it can be observed that the number of studs influences the stiffness of the beams.

The slip between the concrete slab and the steel beam also has been measured (Table 2), both at the stud locations and between the studs. The values vary significantly. The slip value that is compared with the calculation results is the average measured slip. For high loads the calculated slip is larger than the measured slip, and for low loads it is smaller. In general, a reasonable agreement is achieved if the sensitivities of the slip to friction and the local deformation near the studs are taken into account. The low value of the calculated slip at low loads can be explained by excessive stiffness of the connection between concrete and steel at locations close to the midspan, where no slip occurs until the shear flow reaches the value T_1. However, if this portion of the beam were shorter, then its

stiffness at low loads would be too small, as is indeed observed on the load-deflection diagram. At high loads, the calculated slip exceeds the measured values, which shows that the region without slip (located close to the midspan) is smaller and has less influence than the other parts of the response diagram of the study. The acceptable agreement that is seen in the diagrams in Figs. 1(a and b) indicates that a change of the load-slip diagram would probably unfavorably influence the deflection curves, which are the more important results.

Forces and Stresses in Composite Beam

The behavior strongly depends on the geometry of the cross section. The beams used in buildings have rather thick and wide concrete slabs compared with the dimensions of the steel beam. The neutral axis usually lies in the concrete slab. Thus, a part of concrete is under tension, which causes cracking and reduces the stiffness of the slab. The studs are anchored in the tensile zone, and so their stiffness must be expected to be lower than that of the studs anchored in concrete that is under compression. The contribution of the slab to the overall stiffness is high, and the structure is quite sensitive to cracking (as well as to creep and shrinkage).

Bridge beams behave differently. They are rather deep, and the concrete slab is relatively thin. The beams in a bridge are not too far apart, and the width of the slab is comparable with the dimensions of the steel beam. The neutral axis lies normally in the steel part of the cross section. This is advantageous because the slab lies fully in the compression zone. At increasing load, the slab remains elastic above the service load level. The connectors are anchored in the compression zone of the slab, which increases their load-carrying capacity. That is why the bridge beam has been chosen as an example showing the distribution of forces along the composite beam.

The distributions of the bending moments and axial forces in composite beams with deformable and stiff connectors are different. Near the midspan, where the connection is stiff, the total bending moment receives a large contribution from the axial forces in steel and concrete, which forms a couple with the arm c [Fig. 1(top) in Part I]. On the other hand, the connection at the end portion of the beam can be rather weak due to partial failure of connectors, and then the total moment is roughly the sum of the moments in the cross section parts, with a vanishing contribution from the couple of axial forces. These differences cause unusual stress distribution along the beam. The location of the extreme stresses in steel or concrete need not, and normally does not, lie at the midspan.

The bending moment distribution along a half-span is plotted in Fig. 2(a). The total bending moment follows a parabola, as usual, but the bending moment in the steel beam is seen to have a discontinuity at point x_3, at which the slip starts. This discontinuity results from a simplification in the solution, namely, that the v' value at x_3 is nonzero. This discontinuity is caused by assumed sudden slope changes in the approximate force-displacement diagram of the studs (Fig. 3 of Part I) in

TABLE 1. Critical Values of Load-Slip Diagrams of Tested Beams

Beam number (1)	T_1 (kN/m) (2)	T_0 (kN/m) (3)	T_r (kN/m) (4)	v_0 (mm) (5)	v_m (mm) (6)
1 (7 studs)	40.0	85.8	20.0	0.5	5.0
2 (5 studs)	28.6	61.3	14.3	0.5	5.0
3 (4 studs)	22.9	49.0	11.4	0.5	5.0
4 (3 studs)	17.1	36.8	8.6	0.5	5.0

TABLE 2. End Slip between Concrete and Steel (mm)

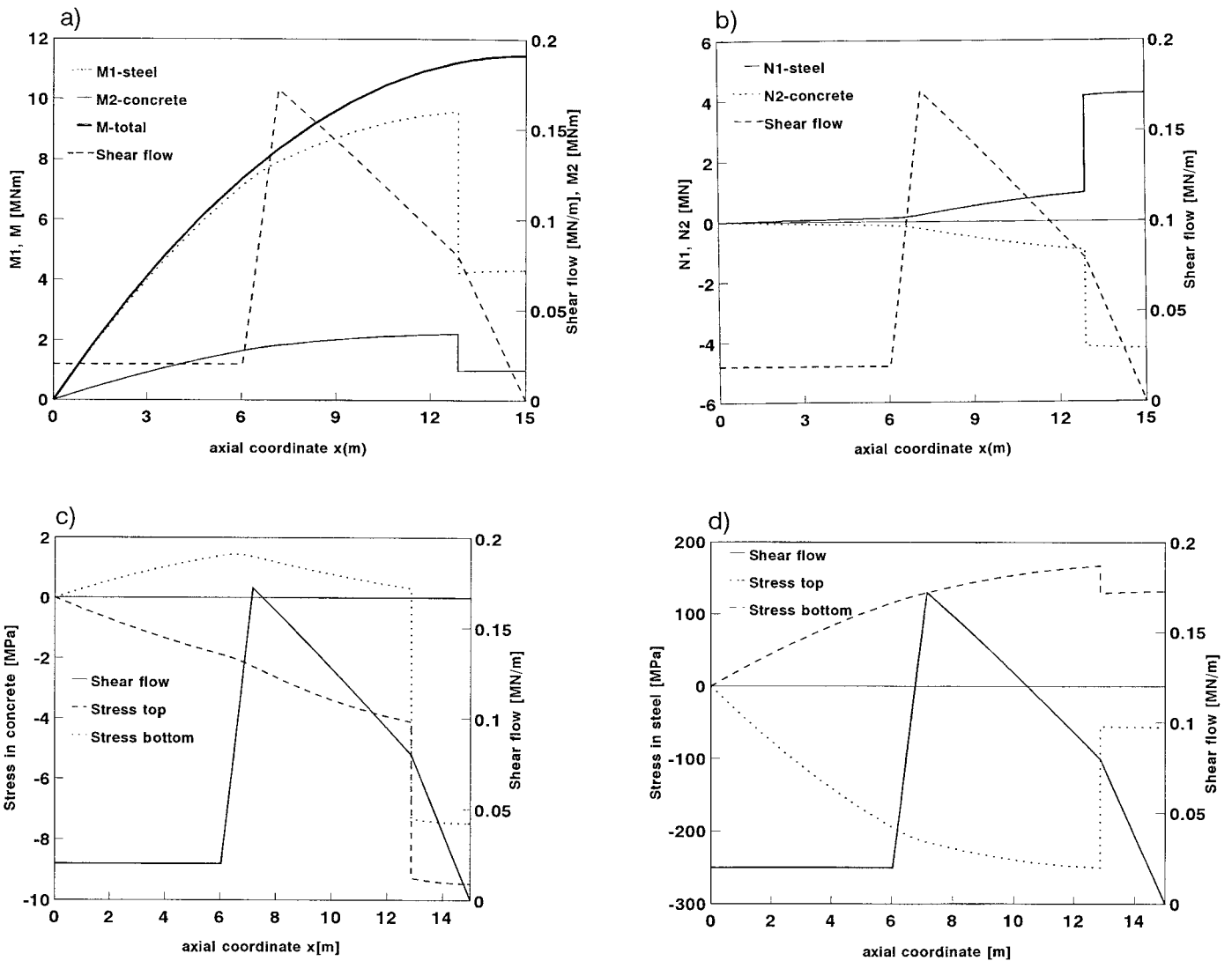| Loading (kN/m²) (1)	Beam 1—7 Studs		Beam 2—5 Studs		Beam 3—4 Studs		Beam 4—3 Studs	
	Experiment (2)	Analysis (3)	Experiment (4)	Analysis (5)	Experiment (6)	Analysis (7)	Experiment (8)	Analysis (9)
5.5	0.65	0.88	—	—	—	—	—	—
5.0	—	—	1.00	1.21	—	—	—	—
4.0	0.35	0.39	0.55	0.64	—	—	—	—
3.5	—	—	—	—	0.50	0.67	—	—
3.0	—	—	0.30	0.36	—	—	—	—
2.5	—	—	—	—	0.30	0.34	0.45	0.48
2.0	0.08	0.04	—	—	—	—	—	—
1.5	—	—	0.10	0.04	0.10	0.09	0.20	0.17

FIG. 2.   (a) and (b) Internal Forces Distribution; (c) and (d) Stress Distribution along Bridge Beam Analyzed

which the shear flow T_1 develops without any slip. In reality, of course, a smooth variation of the bending moments can be expected. The present model indicates a significant drop of the bending moment in the central region of the beam and an increase of the axial force in this region, as seen in Fig. 2(b). For the sake of clarity, the quadrilinear diagram of the shear flow is also plotted in Figs. 2(a and b).

The stress distribution in the concrete part of the cross section is plotted in Fig. 2(c). The compression stress at the top surface reaches its maximum at the midspan, but the tensile stress at the bottom flange reaches its maximum in the region of the descending shear flow-slip diagram, which lies approximately at quarter-span. The stress in steel is distributed similarly as the bending moments in steel, and its extreme value occurs at x_3 [Fig. 2(d)].

The dimensions of the composite bridge beams analyzed and the connector characteristics are summarized in Table 3. The figures show that the behavior of connection affects significantly the distribution of stresses. If the value of T_1 in the shear flow-slip diagram is zero, the stiffness of the beam is reduced dramatically. For $T_1 = 80.0$ kN/m, the deflection of the bridge beam under a distributed load of 101.8 kN/m is about 67.6 mm. For $T_1 = 0$, this deflection increases to 85.2 mm, whereas the maximum stress in the steel moves to the midspan and its value increases from 250.0 to 271.8 MPa. Moderate though the slip is, the connection close to the midspan is nevertheless rather important as well.

TABLE 3.   Dimensions of Beams Analyzed

Parameter (1)	$n = 0.25$ (2)	$n = 1.0$ (3)	$n = 4$ (4)
Depth of steel beam (m)	0.625	2.5	10.0
Thickness of slab (m)	0.05	0.2	0.8
Width of slab (m)	0.625	2.5	10
I_1 (inertia moment) (m⁴)	0.2245E-3	57.474E-3	14.713
I_2 (m⁴)	6.510E-3	1.6667E-3	0.4266
A_1 (cross section area) (m²)	4.226E-3	67.625E-3	1.082
A_2 (m²)	0.3125	0.5	8.0
c_1 (Fig. 1) (m)	0.3955	1.582	6.328
c_2 (Fig. 1) (m)	0.025	0.1	0.4
T_1 (Fig. 3) (kN/m)	20	80	320
T_0 [maximum shear flow (Fig. 3)] (kN/m)	43	172	688
v_0 (slip at maximum shear flow) (mm)	6.8	6.8	6.8
v_m (Fig. 3) (mm)	8.16	8.16	8.16
L (span) (m)	7.5	30	120

If the slope of the initial (prepeak) segment of the shear flow-slip diagram (Fig. 3 of Part I) is gradually increased toward the vertical ($v_0 \rightarrow 0$), point x_3 remains at the midspan. On the other hand, if the initial segment is actually vertical [Fig. 3(b)], point x_3 lies always away from the midspan. Thus the limit case $v_0 \rightarrow 0$ of the diagram in Fig. 3 of Part I for $T_1 > 0$ might not approach the type of response applicable for the
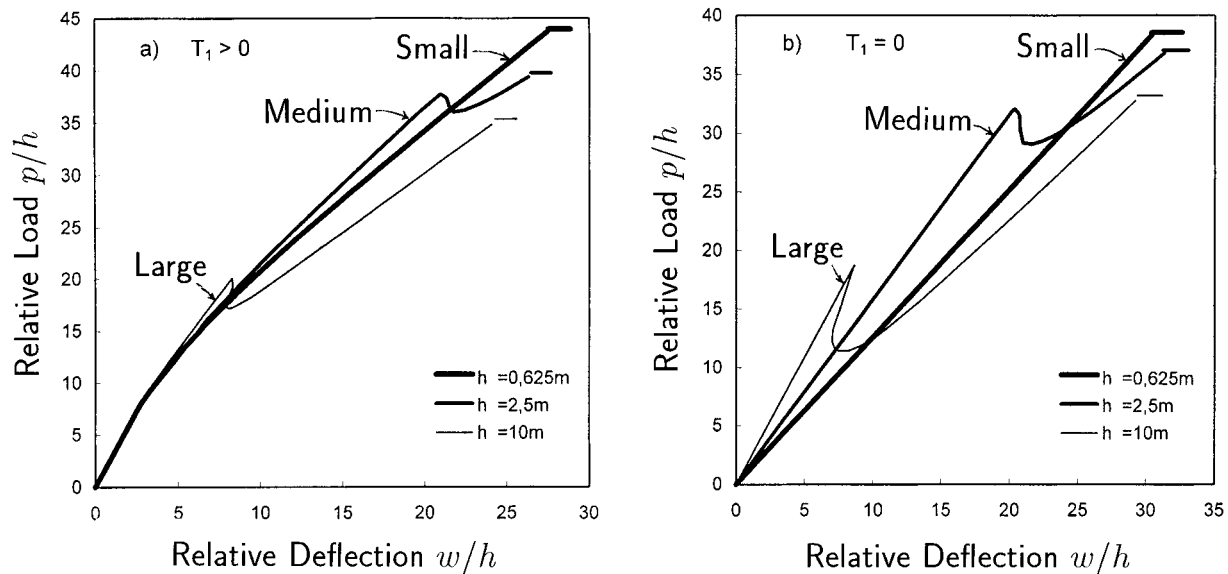
FIG. 3. Load-Deflection Diagram of Bridge Beams for: (a) $T_1 > 0$; (b) $T_1 = 0$

case $T_1 = 0$. Curiously, there is a discontinuity between the responses for these two types of shear flow-slip diagrams.

Behavior and Size Effect

We consider now the scaling of type 1 in which the connectors and the interface area per connector are not scaled with the beam. The nominal strength of the composite beam is now defined as $\sigma_N = p_{max}/h_1$, where h_1 is the depth of the steel beam (i.e., $D = h_1$). The residual load capacity of the beam depends on whether the shear flow-slip diagram (Fig. 3 of Part I) begins by a vertical segment. If this is the case, the residual load capacity is provided by a critical portion of the interface transmitting shear without any slip, whereas the remainder of the interface slips freely. The peak load in this case must satisfy at location x_3 the following condition:

$$T_1 = \frac{V(x_3)Q_{tr}}{I_{tr}} \tag{13}$$

where Q_{tr} and I_{tr} = static (first) moment and the inertia moment of the slab with respect to the centroidal axis of the transformed cross section of the composite beam, respectively. However, the location x_3 and shear force V are unknown. As the second condition it is assumed that the extreme stress in steel

$$\sigma_s = \frac{M_s(x_3)}{I_{tr}} c_1 = 250 \text{ MPa} \tag{14}$$

From the last two conditions, a quadratic equation for x_3 is obtained

$$-\frac{F_1 I_{tr}}{Q_{tr}} x_3^2 + \left(\frac{F_1 I_{tr}}{Q_{tr}} l + \frac{2M_s(x_3)}{k}\right) x_3 - \frac{M_s(x_3)}{k} l = 0 \tag{15}$$

where $k = [1 + (E_2 l_2 / E_1 l_1)]^{-1}$. The residual load p_r is

$$p_r = \frac{2T_1 l_{tr}}{Q_{tr}(l - 2x_3)} \tag{16}$$

The nominal value of the residual stress $\sigma_r = p_r/h_1$.

If the residual shear strength T_r of the connectors vanishes (Fig. 3 of Part I, $T_1 = 0$), the residual load is obtained as the combined load-carrying capacity of the beam and slab with no shear transmitted across the interface. The yield stress in steel, $\sigma_s = 250$ MPa, is reached at the midspan, and so

$$p_r = \frac{8M_s}{l^2} \frac{E_1 l_1 + E_2 l_2}{E_1 l_1} \quad \text{with} \quad M_s = \frac{\sigma_s I_1}{c_1} \tag{17}$$

If the residual shear strength of connectors is finite (Fig. 3 of Part I, $T_1 > 0$), the resulting load-deflection diagrams for the three beam sizes are shown in Fig. 3(a). If the connection reaches softening [i.e., if the slip at the end exceeds v_0 (Fig. 3 of Part I)], there exists a gradually descending portion on the load-deflection diagram. For the smallest beam analyzed, the maximum load is reached because σ_s attains the value 250 MPa, which is before the peak force of connection is attained. For the two larger sizes, the connection begins to soften first and the ultimate load of beam is reached afterward.

The stiffness of connection is not the same for the three sizes. The reason is the assumption that the studs are of the same size and only their spacing (or number per unit length) varies. This assumption gives similarity in the shear flow capacity of the connection but not in the stiffness of the connection. As seen in Fig. 3 of Part I, the load-deflection diagrams of the connectors of the smallest and medium sizes have different shear force values, for the same displacement. (Two noninteracting studs can carry more than twice the load of one study, but the displacement at failure is the same.) The stiffness of the connection is for the larger size $T_{v,large}$ and for the smaller size $T_{v,small}$. The larger specimen, therefore, has a steeper load-displacement diagram than the smaller specimen, which can be seen in Figs. 3(a and b).

The larger the composite beam, the smaller the nominal strength (ultimate nominal stress) $\sigma_N = p_{max}/h$, which represents a size effect. The maximum load, as indicated by the attainment of yield stress $\sigma_s = 250$ MPa, is reached at the end of the curves in Fig. 3(a). The nominal strength (or ultimate stress, against which the design should ensure sufficient safety margin), should be considered, from the practical viewpoint, as the first peak of the load-displacement diagram. Its value is, for larger beam sizes, substantially lower than the subse-

TABLE 4. Ultimate Load (Nominal Stress)

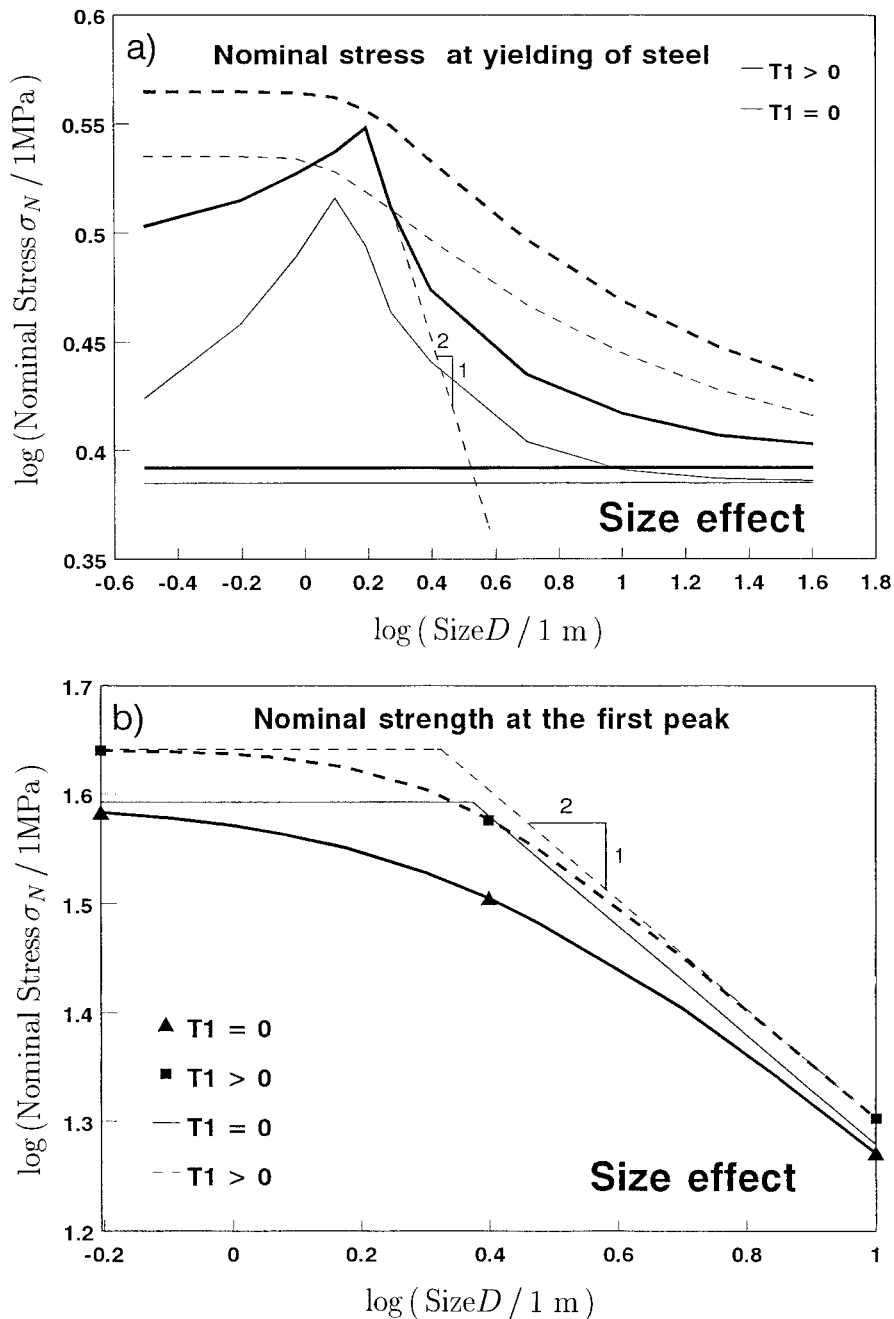| h (1)	Ultimate load ($T_1 > 0$) (2)	First peak load ($T_1 > 0$) (3)	Ultimate load ($T_1 = 0$) (4)	First peak load ($T_1 = 0$) (5)
0.625	43.7	—	38.3	—
2.5	39.4	37.7	36.8	32.0
10	34.8	20.1	32.8	18.7

FIG. 4. Size Effect Obtained from Differential Equations: (a) Nominal Strength at Start of Yielding of Steel Beam; (b) Nominal Strength at First Peak of Load Displacement Diagram

quent maximum value reached (Table 4). In this sense, the decrease of nominal strength with increasing size of the beam is significant.

The load-deflection curves of the beams with connections behaving according to Fig. 3 of Part I with $T_1 = 0$ (no finite vertical segment) are plotted in Fig. 3(b). The features observed in Fig. 3(a) may also be seen here. The increase of the stiffness of the connection with an increasing size is more pronounced here. The nominal strength is lower than in the preceding case ($T_1 > 0$), as may have been expected.

Fig. 4(a) shows the typical diagram of the size effect on the nominal strength of composite beam (for $T_1 > 0$ represented by heavy solid lines and for $T_1 = 0$ represented by light solid lines). The excess of the nominal strength ($\sigma_N = p_{max}/h$) over the residual stress ($\sigma_r = p_r/h$) [horizontal asymptotes in Fig. 4(a)] is plotted versus the beam size in logarithmic scales. For comparison, the dashed lines in Fig. 4(a) show the (approxi-

TABLE 5. Parameters of Size Effect Law

$f'_t = 3.0$ MPa (1)	B (2)	D_0 (3)	r (4)	σ_r (5)
$T_1 > 0$ [Fig. 10(a)]	0.40	1.56	6	2.47
$T_1 = 0$ [Fig. 10(a)]	0.33	1.25	6	2.43
$T_1 > 0$ [Fig. 10(b)]	14.58	2.11	3.54	0
$T_1 = 0$ [Fig. 10(b)]	13.04	2.36	1.86	0

mate) generalized size effect law (with constants B, D_0, and σ_r given in Table 5)

$$\sigma_N = \frac{Bf'_t}{[1 + (D/D_0)^r]^{1/2r}} + \sigma_r \qquad (18)$$

It is interesting that the size effect diagrams have peaks. Only the right-hand portions of the diagrams exhibit the usual decrease of σ_N with increasing D. The peak of the size effect

diagram occurs for a certain critical size D_{cr} for which the steel attains its yield strength simultaneously with the peak shear flow in the studs, which is exactly at the peak of the load-deflection curve. For a larger beam depth, the steel begins to yield only after the peak of the shear flow-slip diagram of the studs. When the beam depth is further increased, the peak on the load-deflection curve (Fig. 3) moves down, and its effect on the overall maximum load (at which the steel yields) becomes lower.

For very large beam sizes the steel begins to yield long after all the studs have failed. It alone decides the maximum load, which corresponds to the case of no shear transfer between steel and concrete. Thus the nominal strength for very large sizes is decided only by the yielding of steel. Hence, the size effect must asymptotically disappear, and a finite residual nominal strength must be approached.

The reverse size effect (i.e., an increase of σ_N with increasing D), which is seen in the left-hand portions of the diagrams in Fig. 3, is at first sight striking. It occurs in the small size range in which the studs do not fail and the maximum load is determined by the yield strength of the steel beam. Because the connection stiffness is lower in smaller beams (Fig. 3 of Part I), the contribution to load capacity is mobilized to a lesser extent in smaller beams, and the steel begins to yield earlier relative to stud failure.

If, however, the ultimate load is assumed as the first peak of the load-deflection diagram [i.e., as the lower of (1) the load at yield limit of steel; or (2) the first peak load] then the usual—decreasing—size effect is obtained. This is documented by Fig. 4(b), in which the residual stress σ_r is not subtracted from the ordinates σ_N because, for larger beam sizes, it is smaller than the nominal strength of the beam calculated under this assumption. The nominal strength for the first peak load for an infinitely large beam seems to approach zero.

Comparison with Energy Release Approach

The size effects obtained by the energy release analysis of the fracture mechanics type and by the direct solution of the differential equations are similar but only qualitatively. A close match is not possible because each is suited for a different range of situations. The solution of differential equations is considerably more complicated than the energy analysis of the problem and does not lead to simple formulas for the size effect. This solution is doubtless more accurate than the energy release analysis of the fracture mechanics type when the zone of failing connectors is long, which happens for normal beam sizes. However, it seems difficult to extract from this solution the asymptotic size effect, which is obtained easily by the energy approach.

A particular difficulty in solving the differential equations is presented by the nonlinearity in solving the location of the cross sections that separate different response regimes of the connectors. This nonlinearity causes convergence difficulties in the present iterative form of solution (and is the reason why a systematic analysis of many cases could not be included in the present funded project due to its very limited scope). Therefore, other alternatives of solution should be explored in the future. As a brute force approach, nonlinear finite-element analysis of the beam with softening connectors may be used to check important designs in practice.

SUMMARY AND CONCLUSIONS

1. The premise of the analysis is that the slip of shear connectors in composite beams exhibits postpeak softening. If postpeak softening of the shear connectors could be completely eliminated, the theory of limit states would apply and no size effect would occur.
2. The nominal strength of composite beams with softening connectors exhibits a strong and complex size effect. Energy release analysis analogous to fracture mechanics may be used to obtain a simple characterization of the size effect suitable for design.
3. The local source of size effect is that the behavior of studs is softening, characterized by a stress-displacement rather than stress-strain relation. The global source of size effect is that the shear forces in the studs localize along the beam, due to the fact that the studs do not fail simultaneously but progressively as the front of stud failures propagates along the beam. The propagation of stud failure may cause a peak in the load-deflection diagram of the beam. This peak, though, need not be the overall maximum.
4. If the studs and the interface area per stud are not scaled with increasing beam size, and if the failure of all studs is considered to represent a failure of the whole beam, the nominal stress at the first load peak approximately follows Bažant's size effect law (1984) [Fig. 4(b)]. When the onset of yielding in steel is considered to represent failure of the composite beam, then the usual decrease of the nominal strength with increasing beam size is obtained only for large enough sizes exceeding a certain critical size, whereas for smaller sizes a reverse size effect may result.
5. In the case of perfect geometric scaling, in which the size of the studs and the interface area per stud are increased with increasing beam size, there is a compound size effect, in which the size effect in the failure of individual studs amplifies the size effect due to the propagation of connector failures along the beam. This amplification causes a size hypereffect for which the large size asymptotic size effect is stronger than in linear elastic failure mechanics. Therefore, if possible, the size of the studs should not be increased with the beam size.
6. When the studs exhibit a large slip or fail, the maximum stress in a simply supported composite beam under a uniform load is reached near the front of the row of failing studs, rather than at the midspan.
7. The way the ultimate load-carrying capacity is reached depends on the size of the beam. For small beams the steel may begin to yield before the studs fail, which is a desirable behavior. But for large enough beams the studs fail before the steel can start yielding. (Stud failures may, of course, engender excessive deflections even for small beams that do not collapse.)
8. Comparison of theoretical predictions with the limited test data that exist in the literature does not indicate any significant disagreement. However, experimental verification and calibration of the size effect in composite beams is needed.
9. *Implications for design:* The size effect on the load capacity, as measured by the nominal strength, must be taken into account if the connection is not strong enough. The connectors should be designed so that, under service loads (the serviceability limit state), no slip would occur, which means that the shear flow should be less than T_1 (and that the load-deflection diagram of the connectors should start with a vertical segment). If some connectors reach their maximum (ultimate) force before the maximum load (ultimate load and load capacity) is attained, the maximum load should be defined as the lower of (1) the minimum immediately after the first peak in Fig. 3 (this peak is associated with the propagation of connector failures and is subjected to size effect; note the two larger

beams in Fig. 3); and (2) the load at which the yield or strength limit in steel or concrete is attained (the smallest beam in Fig. 3). Ideally, the design should be that the maximum shear force would not be reached in any connector before arriving at the maximum load of the beam; that is, the failure should begin by yielding of the steel beam, not by slip of the connectors (but even in this ideal case, the consequence of propagating connector failures is that the larger the beam, the steeper is the postpeak descent of load with increasing deflection).

ACKNOWLEDGMENTS

APPENDIX. REFERENCES

Bažant, Z. P. (1984). ''Size effect in blunt fracture: Concrete, rock, metal.'' *J. Engrg. Mech.*, ASCE, 110(4), 518–535.
Bažant, Z. P., and Vítek, J. L. (1999). ''Compound size effect in composite beams with softening connectors. I: Energy approach.'' *J. Engrg. Mech.*, ASCE, 125(11), 1308–1314.
Wright, H. D., and Francis, R. W. (1990). ''Tests on composite beams with low levels of shear connection.'' *The Struct. Engr.*, London, 68(15/7), 293–298.